

# Neutrino and gravitational wave signal of a delayed-detonation model of Type Ia supernovae

Ivo R. Seitenzahl\*

*Research School of Astronomy and Astrophysics, The Australian National University,  
Cotter Road, Weston Creek, ACT, 2611, Australia*

*ARC Centre of Excellence for All-Sky Astrophysics (CAASTRO)*

*Institut für Theoretische Physik und Astrophysik, Universität Würzburg,*

*Emil-Fischer-Str. 31, D-97074 Würzburg, Germany and*

*Max-Planck-Institut für Astrophysik, Karl-Schwarzschild-Str. 1, D-85741 Garching, Germany*

Matthias Herzog

*Max-Planck-Institut für Astrophysik, Karl-Schwarzschild-Str. 1, D-85741 Garching, Germany*

Ashley J. Ruiter

*Research School of Astronomy and Astrophysics, The Australian National University,  
Cotter Road, Weston Creek, ACT, 2611, Australia*

*ARC Centre of Excellence for All-Sky Astrophysics (CAASTRO) and*

*Max-Planck-Institut für Astrophysik, Karl-Schwarzschild-Str. 1, D-85741 Garching, Germany*

Kai Marquardt, Sebastian T. Ohlmann, and Friedrich K. Röpke

*Zentrum für Astronomie der Universität Heidelberg,*

*Institut für Theoretische Astrophysik, Philosophenweg 12, D-69120 Heidelberg, Germany*

*Institut für Theoretische Physik und Astrophysik, Universität Würzburg,*

*Emil-Fischer-Str. 31, D-97074 Würzburg, Germany and*

*Heidelberger Institut für Theoretische Studien, Schloss-Wolfsbrunnengasse 35, 69118 Heidelberg, Germany*

(Dated: January 26, 2016)

The progenitor system(s) and the explosion mechanism(s) of Type Ia supernovae (SNe Ia) are still under debate. Non-electromagnetic observables, in particular gravitational waves and neutrino emission, of thermonuclear supernovae are a complementary window to light curves and spectra for studying these enigmatic objects. A leading model for SNe Ia is the thermonuclear incineration of a near-Chandrasekhar mass carbon-oxygen white dwarf star in a “delayed-detonation”. We calculate a three-dimensional hydrodynamic explosion for the N100 delayed-detonation model extensively discussed in the literature, taking the dynamical effects of neutrino emission from all important contributing source terms into account. Although neutrinos carry away  $2 \times 10^{49}$  erg of energy, we confirm the common view that neutrino energy losses are dynamically not very important, resulting in only a modest reduction of final kinetic energy by two per cent. We then calculate the gravitational wave signal from the time evolution of the quadrupole moment. Our model radiates  $7 \times 10^{39}$  erg in gravitational waves and the spectrum has a pronounced peak around 0.4 Hz. Depending on viewing angle and polarization, we find that the future space-based gravitational wave missions DECIGO and BBO would be able to detect our source to a distance of  $\sim 1.3$  Mpc. We predict a clear signature of the deflagration-to-detonation transition in the neutrino and the gravitational wave signals. If observed, such a feature would be a strong indicator of the realization of delayed-detonations in near-Chandrasekhar mass white dwarfs.

PACS numbers: PACS numbers: 04.30.Db, 04.30.Tv, 26.50.+x, 97.60.Bw

## I. INTRODUCTION

The nature of the progenitor system(s) and the explosion mechanism(s) of Type Ia supernovae (SNe Ia) are still under debate. Although synthetic observables such as time dependent spectra or light curves have been calculated for numerous explosion models [e.g. 1–5], efforts aimed at unambiguously identifying the explosion scenario based on a comparison of the model spectral evo-

lution to observations remain inconclusive [6]. The same holds for the *reverse* process of inferring the composition profile of the supernova using the technique of abundance tomography [7–10]. Complementary approaches aimed at distinguishing the nature of the progenitor systems include the search for the contribution to the early-time light curve from a possible companion [11–13], Na I D line absorption features interpreted as evidence for circumstellar material [14–16], late-time bolometric light curves [6, 17, 18], gamma-ray emission [19–21], setting upper limits on the single degenerate scenario in old stellar populations from the lack of X-ray flux associated with the accretion [22], comparing predictions of SN Ia progeni-

---

\* ivo.seitenzahl@anu.edu.au

tor models with the properties of observed SN remnants [23, 24], searching for the companion stars around young supernova remnants [25–27], or constraining the circumstellar medium and hence the evolutionary channel from radio observations [28, 29]. Another approach aims at constraining the scenarios via rates and delay times, either by comparing prediction of binary population synthesis to observations [30–36] or by inferring e.g. merger rates from the statistics of observed WD binary systems [37].

In this work, we determine and discuss the neutrino and the gravitational wave signal of the N100 explosion model of Seitenzahl et al. [38]. N100 is a recent, state-of-the-art, three-dimensional hydrodynamic explosion model of a delayed-detonation in a near Chandrasekhar-mass ( $M_{\text{Ch}}$ ) carbon-oxygen (CO) white dwarf (WD). Such delayed-detonation models are among the most promising candidates to explain a substantial fraction of the SN Ia population [e.g. 39].

We have chosen the N100 model for our study since its synthetic light curves and spectra make it a rather promising candidate for a “normal” SN Ia [5]. Furthermore, the nucleosynthetic yields and electromagnetic emission of the N100 model have already been used as representative of near- $M_{\text{Ch}}$  delayed-detonations in the single degenerate scenario in several recent publications [6, 21, 40–42]. We emphasize that we actually re-calculate the N100 model from Seitenzahl et al. [38], this time also taking internal energy losses due to neutrino escape from all contributing source terms dynamically into account. For completeness, we therefore refer to this model hereafter as N100 $\nu$ .

## II. NEUTRINO SIGNAL

The maximum central density of WDs is  $\rho_c^{\text{max}} \lesssim 1 \times 10^{10} \text{ g cm}^{-3}$  [see e.g. 43]. Neutrino trapping starts only at densities of  $\sim 10^{11}$  to  $10^{12} \text{ g cm}^{-3}$  [44], WD matter is therefore always transparent to neutrinos; in good approximation, they leave the star without any interaction. This simplifies the neutrino physics greatly, because we can assume that the energy that the neutrinos get when they are created is immediately lost to the star. Nevertheless, in the hot ashes of burnt CO matter, the thermodynamic conditions are such that copious amounts of neutrinos can be emitted. Calculations of the neutrino signal for a few SN Ia explosion models have been presented in the literature. Nomoto et al. [45] and Kunugise and Iwamoto [46] calculated the neutrino signal for the W7 model [45], a one-dimensional fast deflagration of a  $\sim 1.37 M_{\odot}$  CO WD. Odrzywolek and Plewa [47] calculated the neutrino signal for the n7d1r10t15c model [48], a two-dimensional pure deflagration of a  $\sim 1.36 M_{\odot}$  CO WD and the Y12 model [48], a two-dimensional “detonating-failed-deflagration” (gravitationally confined detonation) model of the same  $1.36 M_{\odot}$  CO WD. Although Odrzywolek and Plewa [47] refer

to the Y12 model as a delayed-detonation, this term is usually reserved for SNe Ia that undergo a deflagration-to-detonation transition (DDT) when the deflagration flame front reaches lower densities where it gets shredded by turbulence and the mixing of cold fuel and hot ash triggers a detonation [49]. The explosion mechanism in the Y12 model is fundamentally different in that the detonation is triggered not during the rising phase of the deflagration, but rather at a much later time when deflagration ashes that are gravitationally bound to the surface of the WD collide, see Plewa et al. [e.g. 50], Seitenzahl et al. [e.g. 51].

Previously considered multi-dimensional SN Ia models represent only peculiar events, i.e. pure turbulent deflagration and gravitationally confined detonation models. Here, we present neutrino luminosities for a three-dimensional delayed-detonation model of a  $\sim 1.40 M_{\odot}$  CO WD that underwent a DDT. These explosion models have been extensively studied in the literature, and may be able to explain “normal” SNe Ia [e.g. 5, 52]. For details about our implementation of the DDT model see Ciaraldi-Schoolmann et al. [53]. We distinguish between *weak* neutrinos produced in nuclear reactions and *thermal* neutrinos produced by thermal plasma processes. In the following two sections, we introduce the physical processes that generate the neutrinos during thermonuclear burning in WDs.

### A. Weak neutrinos

*Weak neutrinos* are emitted in nuclear reactions involving the weak interaction<sup>1</sup>; the amount of emitted energy depends on specific reaction rates and therefore on the composition of the matter. The reaction rates themselves depend strongly on temperature and density. Weak neutrinos and antineutrinos are produced in electron captures

$$p + e^- \rightarrow n + \nu_e, \quad (1)$$

positron capture processes

$$n + e^+ \rightarrow p + \bar{\nu}_e, \quad (2)$$

$\beta^+$  decays

$$p \rightarrow n + e^+ + \nu_e, \quad (3)$$

and  $\beta^-$  decays

$$n \rightarrow p + e^- + \bar{\nu}_e. \quad (4)$$

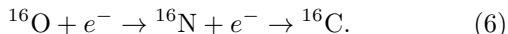
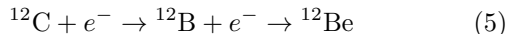
All reactions, which can also occur inside nuclei, change the electron fraction  $Y_e$  (defined as the number of electrons per baryon) of the matter.

<sup>1</sup> Of course, also “thermal” neutrinos are created due to the weak interaction, but their production does not involve nuclear reactions.

Neutrinos from electron captures (1) are abundantly produced in the neutronization processes that take place during and immediately after thermonuclear burning. As we will see, the energy released in reactions (1–4) dominates the energy released in all other neutrino generating processes in the physical environment of thermonuclear supernovae.

In particular, electron capture reactions (1) play an important role during the thermonuclear burning of WD matter. They lead to neutronization, expressed as decreasing  $Y_e$ , lowering the electron degeneracy pressure and thereby affecting the dynamics of the fluid.

Electron captures on the constituent parts of CO WDs,  $^{12}\text{C}$  and  $^{16}\text{O}$ , would occur via the following reactions [54]:



The threshold energy for the first reaction chain is 13.37 MeV, for the second reaction chain 10.42 MeV. The Fermi energies of the electrons match these values at densities of  $\rho_{\text{ec,C}} = 3.9 \times 10^{10} \text{ g cm}^{-3}$  and  $\rho_{\text{ec,O}} = 1.9 \times 10^{10} \text{ g cm}^{-3}$ , respectively [54].

As mentioned above, central densities of accreting CO WDs are not expected to exceed  $\rho_c \sim 9 \times 10^9 \text{ g cm}^{-3}$  [43, 55], well below  $\rho_{\text{ec,C}}$  and  $\rho_{\text{ec,O}}$ , before thermonuclear burning starts in the central region. Therefore, for densities appropriate for CO WDs, no electron captures on the most abundant unburnt nuclei occur. They are only possible after the start of thermonuclear burning, in particular on the hot “ashes”.

Using the weak interaction rates of Langanke and Martínez-Pinedo [56], Seitenzahl et al. [57] calculated extensive tables of the time rate of change of the specific energy  $\dot{E}_\nu$  and the time rate of change of the electron fraction  $\dot{Y}_e$  in these ashes for a three dimensional grid in density, temperature, and  $Y_e$ . We have extended their tables to determine the mean electron neutrino and electron antineutrino energies by implementing equation 17 of Langanke and Martínez-Pinedo [56] into the nuclear statistical equilibrium code of Seitenzahl et al. [57]. We interpolate in the tables to determine the amount of energy carried away by weak neutrinos for each grid cell and simply subtract it from the internal energy of the cell in every time step. The mean neutrino energies are determined by post-processing the output of the hydrodynamics simulations, once again interpolating in the tables, utilizing the NSE mass fraction, electron fraction, temperature, and density stored for each cell.

## B. Thermal neutrinos

In the hot plasmas of stellar interiors, neutrinos are also emitted due to processes that are independent of nuclear reactions; the amount of emitted energy depends only on the density and temperature of the matter. Most important are neutrinos originating from electron-

positron pair annihilation, photoemission, plasmon decay, bremsstrahlung, and recombination processes (for a brief description and summary of the individual contributions of these processes see [58]). Neutrinos from these processes are often combined as *thermal neutrinos*, they comprise neutrinos and antineutrinos of all flavors, whereas in reactions (1–4) only electron and anti-electron neutrinos are produced.

We calculate the energy that is released from the WD due to the emission of *thermal neutrinos* using a code<sup>2</sup> in which analytic fitting formulas from Itoh et al. [58] are implemented. In every time step we simply subtract the resulting locally calculated neutrino energies from the internal energy of each cell.

## C. Results and Discussion

The weak- and thermal neutrino luminosities for N100 $\nu$  are shown as a function of time in Fig. 1. The weak neutrino luminosity reaches a maximum of  $4.74 \times 10^{49} \text{ erg s}^{-1}$  at  $t = 0.53 \text{ s}$  and the integrated total weak neutrino energy loss amounts to  $1.95 \times 10^{49} \text{ erg}$ . The weak neutrino luminosity is overwhelmingly dominated by electron neutrinos from electron captures and  $\beta^+$  decay. In comparison, the electron antineutrino luminosity from positron capture and  $\beta^-$  decay is more than six orders of magnitude smaller (see Fig. 1). At the time of maximum luminosity, the mean weak electron neutrino energy is 4.0 MeV and the mean weak electron antineutrino energy is 2.2 MeV (see Fig. 2). The thermal neutrino luminosity reaches a maximum of  $1.56 \times 10^{47} \text{ erg s}^{-1}$  at  $t = 0.87 \text{ s}$  and the integrated total thermal neutrino energy loss amounts to  $8.70 \times 10^{46} \text{ erg}$ . The energy drained from the explosion by neutrinos is therefore small compared to e.g. the nuclear energy released in the explosion, the initial gravitational binding energy, or the final kinetic energy.

Owing to the stochastic nature of our implementation of the deflagration-to-detonation transition (cf. [53]), even a small additional energy loss could, in principle, lead to very different final explosion. This is, however, not the case here as the time at which the first DDT occurs is only slightly delayed ( $t_{\text{N100}}^{1st\text{DDT}} = 0.928 \text{ s}$  vs.  $t_{\text{N100}\nu}^{1st\text{DDT}} = 0.958 \text{ s}$ ). As a result, there is only a small reduction in kinetic energy between N100 ( $E_{\text{kin}} = 1.45 \times 10^{51} \text{ erg}$ ) and N100 $\nu$  ( $E_{\text{kin}} = 1.42 \times 10^{51} \text{ erg}$ ). Although dynamically not very important, it is interesting to note that the energy carried away by neutrinos in  $\sim 1 \text{ s}$  is still on the same order of magnitude as the total energy radiated in photons by the SN during its entire duration.

The secondary peak around 1.3 s in both the weak and thermal component of the neutrino signal is a signature of the deflagration-to-detonation transition. The

<sup>2</sup> [http://cococubed.asu.edu/code\\_pages/nuloss.shtml](http://cococubed.asu.edu/code_pages/nuloss.shtml)

secondary maximum occurs with a time delay with respect to  $t_{N100\nu}^{1^{st}DDT}$  since the increased neutrino emission occurs only when the detonation (which was launched at low density) overruns the highest density fuel in the center that was left unburned by the deflagration. Odrzywolek and Plewa [47] also find a secondary maximum for the Y12 model and call it a “smoking gun” of delayed-detonation SNe. Their secondary maximum, however, occurs with a relatively long time delay ( $\delta t \gtrsim 3$  s) after the primary maximum. This difference of the occurrence time of the secondary maximum is a reflection of the fundamentally different mechanisms that lead to the initiation of the detonation in the Y12 and N100 $\nu$  models. For a similar reason, these two models also differ by a factor of  $\sim 6$  in their maximum neutrino luminosities,  $L_v^{max}(\text{Y12}) = 8.2 \times 10^{48} \text{ erg s}^{-1}$  vs.  $L_v^{max}(\text{N100}\nu) = 4.7 \times 10^{49} \text{ erg s}^{-1}$ . Although both Y12 and N100 $\nu$  contain both a deflagration and a subsequent detonation, the fact that N100 $\nu$  burns significantly more mass than Y12 during the (for neutrino emission dominant) deflagration phase leads to the fact that the N100 $\nu$  neutrino signal is more like that of pure deflagration models ( $L_v^{max}(\text{n7d1r10t15c}) = 3.9 \times 10^{49} \text{ erg s}^{-1}$  [47],  $L_v^{max}(\text{W7}) = 7 \times 10^{49} \text{ erg s}^{-1}$  [45]), which, however, lack the characteristic secondary maximum of our simulations.

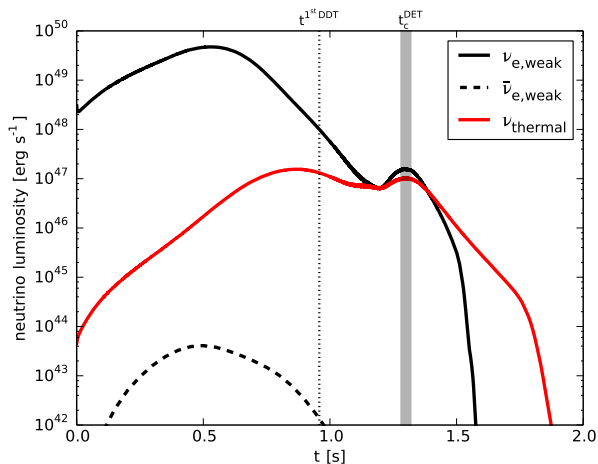


FIG. 1. Neutrino luminosity of the N100 $\nu$  model as a function of time, originating from weak and thermal neutrinos, respectively. Indicated are the time of the first deflagration-to-detonation transition  $t^{1^{st}DDT}$  and the time  $t_c^{DET}$  when the detonation wave reaches the center of the WD.

### III. GRAVITATIONAL WAVE SIGNAL

Research on gravitational wave signals of SNe Ia is a largely unexplored field. A large number ( $\sim 10^4$ ) Galactic binary systems – mostly double white dwarfs – are expected to be resolved with future space-based gravi-

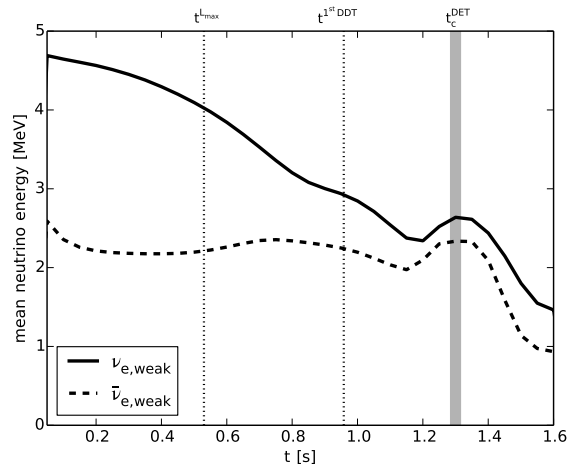


FIG. 2. Mean weak neutrino energies of the N100 $\nu$  model as a function of time, originating from weak  $\nu_e$  and  $\bar{\nu}_e$ , respectively. Indicated are the time of maximum weak neutrino luminosity  $t^{L_{max}}$ , the time of the first deflagration-to-detonation transition  $t^{1^{st}DDT}$ , and the time  $t_c^{DET}$  when the detonation wave reaches the center of the WD.

tational wave observatories such as *eLISA* [59]. Both Nelemans et al. [60] and Ruiter et al. [61] predicted there are about 500 Galactic double degenerate SNe Ia progenitors<sup>3</sup> that harbour the physical properties (distance, mass, separation) to enable their detection in gravitational waves. Dan et al. [62] calculated the gravitational wave signal of a close binary system of two WDs in the ringdown phase until the start of the merger, but they did not model the following thermonuclear burning which may lead to a supernova. Pioneering work on the signal from an actual explosion has recently been performed by Falta et al. [63] and Falta and Fisher [64], who calculated the gravitational wave signal of *gravitationally-confined detonation (GCD)* models of thermonuclear supernovae (the Y12 model discussed extensively in Sec. II falls into this category). In these models, an off-center ignited deflagration bubble rises due to buoyancy forces until it reaches the surface of the WD; the deflagration does not unbind the star but triggers a subsequent detonation that ignites opposite to the point where the deflagration bubble reaches the surface. This scenario leads to asymmetric explosions and thus to relatively strong gravitational wave signals, which are discussed in detail in [63].

Based on their earlier results, [64] analyzed the stochastic gravitational wave background originating from thermonuclear supernovae arising from the gravitational confined detonation explosion mechanism. They found that it might pose a considerable source of noise

<sup>3</sup> These double CO white dwarf systems are assumed to be SNe Ia progenitors because their combined mass exceeds the Chandrasekhar mass limit and they are expected to merge within a Hubble time.

– in the frequency range between 0.1 Hz and 10 Hz – for future gravitational wave detectors such as DECIGO and BBO [65, 66] that are designed to detect the gravitational wave signal of cosmological inflation.

### A. Numerical implementation

Our numerical approach for the computation of the gravitational wave signal follows Blanchet et al. [67] and Müller and Janka [68]. We calculate only the approximate *quadrupole radiation* because of the Newtonian nature of our simulations.

The most straightforward way to determine the amplitude of gravitational quadrupole waves is by calculating the second derivative of the quadrupole moment  $\mathbf{Q}$ . The gravitational quadrupole radiation field in the transverse-traceless gauge  $\mathbf{h}^{\text{TT}}$  is

$$h_{ij}^{\text{TT}}(\mathbf{x}, t) = \frac{2G}{c^4 D} P_{ijkl}(\mathbf{n}) \frac{\partial^2}{\partial t^2} Q_{kl} \left( t - \frac{D}{c} \right). \quad (7)$$

$\mathbf{P}$  is the transverse-traceless projection operator

$$P_{ijkl}(\mathbf{n}) = (\delta_{ik} - n_i n_k) (\delta_{jl} - n_j n_l) - \frac{1}{2} (\delta_{ij} - n_i n_j) (\delta_{kl} - n_k n_l), \quad (8)$$

with the normalized position vector  $\mathbf{n} = \mathbf{x}/D$  and the distance to the source  $D = |\mathbf{x}|$ . However, the calculation of the second time derivative gives rise to numerical instabilities, the resulting signal is quite noisy. Therefore, to avoid this unfavorable method, Nakamura and Oohara [69] and Blanchet et al. [67] introduced a different way to compute the amplitude. With this new method, which was applied successfully to core-collapse supernovae by Moenchmeyer et al. [70] and Müller and Janka [68], the gravitational quadrupole radiation field  $\mathbf{h}^{\text{TT}}$  is calculated by

$$h_{ij}^{\text{TT}}(\mathbf{x}, t) = \frac{2G}{c^4 R} P_{ijkl}(\mathbf{n}) \int d^3x \rho (2v_k v_l - x_k \partial_l \Phi - x_l \partial_k \Phi). \quad (9)$$

Here  $\mathbf{v}$  is the velocity and  $\Phi$  is the usual Newtonian gravitational potential or an effective relativistic gravitational potential. Blanchet et al. [67] showed that equation (10) is equivalent to equation (7), while Moenchmeyer et al. [70] demonstrated the numerical superiority of the method that implements equation (10).

Since gravitational waves have two polarization states (“+” and “×”), the amplitude can be written in terms of the two *unit linear-polarization tensors*  $\mathbf{e}_+$  and  $\mathbf{e}_\times$  [71] as

$$h_{ij}^{\text{TT}}(\mathbf{x}, t) = \frac{1}{R} (A_+ \mathbf{e}_+ + A_\times \mathbf{e}_\times). \quad (10)$$

In the case of a plane wave propagating in  $z$ -direction, the unit linear-polarization tensors are

$$\mathbf{e}_+ = \mathbf{e}_x \otimes \mathbf{e}_x - \mathbf{e}_y \otimes \mathbf{e}_y \quad (11)$$

$$\mathbf{e}_\times = \mathbf{e}_x \otimes \mathbf{e}_y + \mathbf{e}_y \otimes \mathbf{e}_x, \quad (12)$$

where  $\mathbf{e}_x$  and  $\mathbf{e}_y$  are the unit vectors parallel to the  $x$ - and  $y$ -axis, respectively. We calculate the amplitudes  $A_+$  and  $A_\times$  considering two different lines of sight, as was suggested in Müller and Janka [68]. Since they use preferentially spherical coordinates, they speak of the polar ( $\vartheta = 0, \varphi = 0$ ) and equatorial ( $\vartheta = \pi/2, \varphi = 0$ ) direction. In our case, as we use exclusively Cartesian coordinates, it is more appropriate to call it the  $z$ -direction and  $x$ -direction, which we do from now on. With the definition

$$A_{ij} = \frac{G}{c^4} \int d^3x \rho (2v_i v_j - x_i \partial_j \Phi - x_j \partial_i \Phi), \quad (13)$$

the amplitudes  $A_+$  and  $A_\times$  in the  $z$ -direction can be expressed as

$$A_+^z = A_{xx} - A_{yy} \quad (14)$$

$$A_\times^z = 2A_{xy}, \quad (15)$$

while in the  $x$ -direction one obtains

$$A_+^x = A_{zz} - A_{yy} \quad (16)$$

$$A_\times^x = -2A_{yz}. \quad (17)$$

We implemented the calculation of these amplitudes according to equation (13) in the simulation code. Next we show results of the calculated gravitational wave signal, beginning with a discussion of the four amplitudes (14–17).

### B. Gravitational wave amplitudes

In Fig. 3 we plot four different gravitational wave amplitudes that arise from two different lines of sight ( $x$ - and  $z$ -direction), each with two polarization states ( $\times$  and  $+$ ), see Sec. III A for a detailed explanation. In the first  $\sim 0.4$  s after the ignition of the deflagration, no signal is visible; after that the absolute values of all amplitudes rise in a steady, monotonic way. The initiation of the first detonation at  $t^{\text{st}DDT} = 0.958$  s and the time  $t_c^{\text{DET}} \sim 1.3$  s when the detonation reaches the center of the WD leave visible imprints on the signal. For  $A_+^x$ , the signal reaches a maximum value of  $hD \sim 4$  cm at  $t \sim 1.36$  s, about a factor of 3 less than the maximum amplitude obtained by [63] in their GCD model. The smaller maximum amplitude of the N100 $\nu$  delayed-detonation model is naturally explained by the greater compactness of the GCD model when the detonation is triggered. The homologous expansion of the supernova ejecta after  $\sim 3$  s generates a signal that is constant in time up to  $t = 100$  s, when the simulation was stopped.

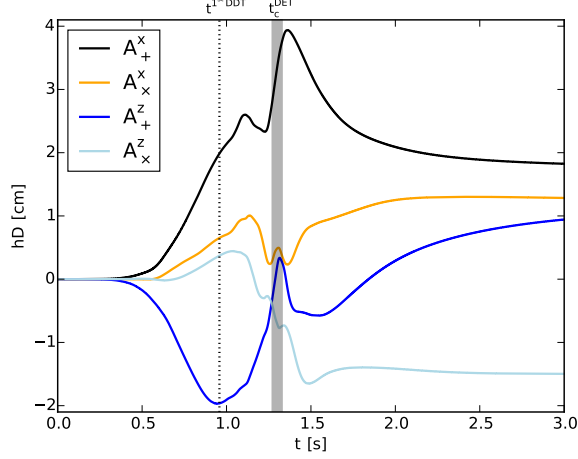


FIG. 3. Time evolution of four gravitational wave amplitudes for the delayed-detonation model N100 $\nu$ , see text for details. Indicated are the time of the first deflagration-to-detonation transition  $t^{1st DDT}$  and the time  $t_c^{DET}$  when the detonation wave reaches the center of the WD.

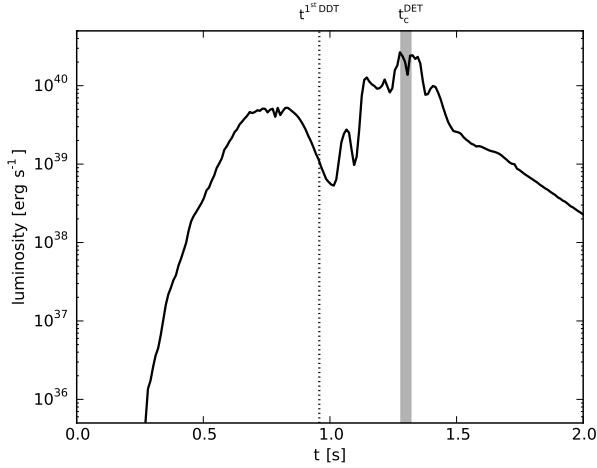


FIG. 4. Gravitational wave luminosity as a function of time of the delayed-detonation model N100 $\nu$ . Indicated are the time of the first deflagration-to-detonation transition  $t^{1st DDT}$  and the time  $t_c^{DET}$  when the detonation wave reaches the center of the WD.

### C. Gravitational wave luminosity and spectrum

Beyond the amplitudes, another quantity of interest is the total amount of energy radiated away by gravitational

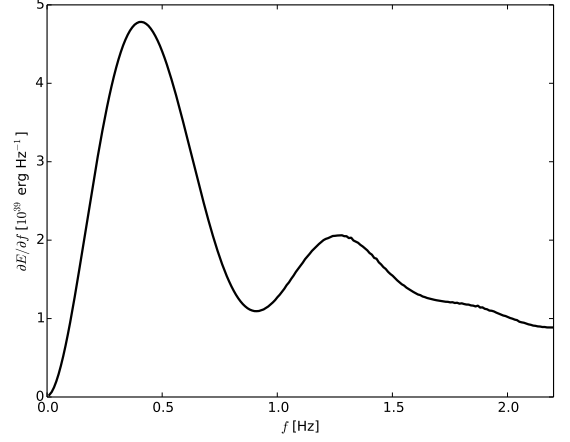


FIG. 5. Energy spectrum of the gravitational wave signal of the delayed-detonation model N100 $\nu$ .

waves,  $E_{gw}$ . It can be expressed as [68]

$$\begin{aligned}
 E_{gw} &= \frac{2c^3}{5G} \int_{-\infty}^{+\infty} \left( \frac{d}{dt} \left( A_{ij} - \frac{1}{3} \delta_{ij} A_{kk} \right) \right)^2 dt \\
 &= \frac{2c^3}{15G} \int_{-\infty}^{+\infty} \left( \dot{A}_{xx}^2 + \dot{A}_{yy}^2 + \dot{A}_{zz}^2 - \dot{A}_{xx}\dot{A}_{yy} - \dot{A}_{xx}\dot{A}_{zz} \right. \\
 &\quad \left. - \dot{A}_{yy}\dot{A}_{zz} + 3 \left( \dot{A}_{xy}^2 + \dot{A}_{xz}^2 + \dot{A}_{yz}^2 \right) \right) dt.
 \end{aligned} \tag{18}$$

All values of  $E_{gw}$  stated in this work are calculated by means of equation (18).

The total gravitational wave energy of N100 $\nu$  amounts to  $6.9 \times 10^{39}$  erg, about an order of magnitude less than the total energy of the GCD model of Falta et al. [63] – this is again consistent with the results shown in Sec. IIIB, because the calculated amplitudes differ by a factor of  $\sim 3$  and the energy is proportional to the square of the amplitudes. These results demonstrate that the gravitational wave energy is dynamically unimportant since it is smaller than the internal-, kinetic-, nuclear-, and even neutrino loss energies. Hence, the error caused by the fact that we did not couple the gravitational waves part of the code to the hydrodynamics part is negligible.

The gravitational wave luminosity as a function of time is plotted in Fig. 4. Clearly visible is a two-peaked structure; the first peak corresponds to the deflagration phase and features a maximum luminosity of  $8 \times 10^{39}$  erg s $^{-1}$  at  $t \sim 0.8$  s, while the second, considerably higher peak can be attributed to the detonation phase, peaking at the time  $t_c^{DET} \sim 1.3$  s when the detonation reaches the center of the WD and converts the last remaining high density fuel to iron group elements. Here the maximum luminosity is  $3 \times 10^{40}$  erg s $^{-1}$ . In contrast, the GCD model of Falta et al. [63] predicts a much greater difference in maximum power radiated in the deflagration and detonation phases. This difference is due to the more weakly

ignited deflagration, which leads to a smaller degree of expansion and correspondingly a detonation in a more compact WD.

The *frequency*  $f$  of a gravitational wave signal is an important quantity to determine, because detectors are only sensitive in a confined frequency range; see [72] for a discussion on quantifying gravitational wave source amplitude and sensitivity curves. We adopt the approach of Müller [73] and Müller et al. [74] and conduct Fourier analyses of the calculated gravitational wave amplitudes and determine the energy spectrum  $\partial E_{gw}/\partial f$ . The Fourier transforms of the  $A_{ij}(t)$  are

$$\tilde{A}_{ij}(f) = \int_{-\infty}^{\infty} A_{ij}(t) e^{2\pi i f t} dt. \quad (19)$$

Following Müller et al. [74], we obtain the energy spectrum by

$$\begin{aligned} \frac{\partial E_{gw}}{\partial f} = \frac{2c^3}{15G} (2\pi f)^2 & \left( \left| \tilde{A}_{xx} - \tilde{A}_{yy} \right|^2 + \left| \tilde{A}_{xx} - \tilde{A}_{zz} \right|^2 + \right. \\ & \left. \left| \tilde{A}_{yy} - \tilde{A}_{zz} \right|^2 + 6 \left( \left| \tilde{A}_{xy} \right|^2 + \left| \tilde{A}_{xz} \right|^2 + \left| \tilde{A}_{yz} \right|^2 \right) \right) \end{aligned} \quad (20)$$

Fig. 5 shows the energy spectrum of the gravitational wave signal, calculated by means of equation (20) by evaluating the Fourier integrals (19). The spectrum has a pronounced maximum of  $4.8 \times 10^{39} \text{ erg s}^{-1}$  at  $f_{max} = 0.41 \text{ Hz}$  and a secondary local maximum of  $2.1 \times 10^{39} \text{ erg s}^{-1}$  at  $1.28 \text{ Hz}$ .

The energy spectrum calculated by [63] for the GCD model peaked at  $\sim 2 \text{ Hz}$ . It is worth noting that Falta et al. [63] stated that an explosion model with more “pre-expansion” prior to detonation, such as the N100 $\nu$  model presented here, would exhibit a characteristic gravitational wave frequency shifted downward by a factor of  $\sim 2$ , a prediction that we essentially confirm.

#### D. Discussion

Our results show that the detection of gravitational wave signals of SNe Ia provides a way to differentiate between different explosion models with future gravitational wave observatories, if data analysis techniques are developed to extract those signals. The signal of our explosion model bears the mark of the deflagration-to-detonation transition. Gravitational waves generated by mergers of two WDs would feature the characteristic signature of the ringdown phase – according to Dan et al. [62], the gravitational wave signal in the ringdown phase is of the same magnitude as the signal of the supernova in the above discussed scenarios:  $hD = 2 \text{ cm}$  to  $20 \text{ cm}$ , depending on the WD masses. Finally, GCD models show a sharp single peak in the time evolution of the amplitude (figure 2 in Falta et al. 63). However, the low

frequency range of the signals prevents a detection by second-generation instruments comparable to advanced LIGO; but third-generation space-based detectors like BBO or DECIGO that cover a lower frequency range should be able to detect the gravitational wave signal of at least all Galactic Type Ia supernovae.

The gravitational wave frequencies that we obtain are consistent with the results of Falta et al. [63] and Falta and Fisher [64]. Our results show that also thermonuclear supernovae modeled as delayed detonations contribute to the stochastic gravitational wave background in the frequency range between  $0.1 \text{ Hz}$  and  $10 \text{ Hz}$  and thus pose a source of noise that might obscure the gravitational wave signal originating from the era of inflation shortly after the Big Bang; the measurement of this signal is a central goal of the planned detectors BBO and DECIGO.

Finally, we estimate the detectability of our N100 $\nu$  delayed-detonation model. Depending on viewing angle and polarization, our gravitational wave amplitudes fall in the range between approximately  $1$  to  $4 \text{ cm}$  (see Fig. 3). At  $\sim 1 \text{ Hz}$ , both BBO and DECIGO have a planned strain sensitivity limit of  $h_{min} \approx 10^{-24}$  [72]. Setting  $D_{max} = hD/h_{min}$  we find that our model’s signal would be detectable out to a distance of  $320 \text{ kpc}$  and  $1.3 \text{ Mpc}$  for  $A_{\times}^x$  and  $A_{+}^x$ , respectively. Thus, a delayed-detonation SN Ia going off in our Milky Way or one of its satellite galaxies would be well within the sensitivity limits of BBO or DECIGO. For fortuitous alignment (i.e.  $A_{+}^x$ ), even the Triangulum and Andromeda galaxies ( $\sim 900 \text{ kpc}$  and  $\sim 780 \text{ kpc}$ , respectively) would be within reach.

#### IV. CONCLUSIONS

We conducted a three-dimensional hydrodynamic simulation of a delayed-detonation explosion of a thermonuclear supernova and computed the neutrino and gravitational wave signals. By taking the energetics of neutrino losses on the hydrodynamic evolution into account, we find a reduction in kinetic energy of about two per cent and we conclude that the effects of neutrino emission on the explosion dynamics are indeed small. Nevertheless, our model emits  $2 \times 10^{49} \text{ erg}$  in neutrinos, comparable to the total energy radiated by photons. We present the amplitudes, luminosity as a function of time, and the energy spectrum of the gravitational wave signal of our SN Ia supernova explosion simulation. The energy spectrum of the gravitational wave emission peaks where the proposed space-based gravitational wave missions DECIGO and BBO have the highest design sensitivity and we find that the signal is potentially observable out to a distance of  $1.3 \text{ Mpc}$ . In both the neutrino and gravitational wave signals we find a distinct signature of the deflagration-to-detonation transition, which, in principle, makes it possible to constrain the explosion model of SNe Ia by observations of their non-electromagnetic

neutrino and/gravitational wave radiation.

## ACKNOWLEDGMENTS

We thank Christopher Moore for his insightful comments on sensitivity curves of gravitational wave detectors and Rüdiger Pakmor for their discussions on power spectra and Fourier transforms. IRS was funded by the Australian Research Council Laureate Grant FL0992131 and the Deutsche Forschungsgemeinschaft (DFG) through the graduate school on “Theoretical Astrophysics and Particle Physics” (GRK 1147), MH by CompStar, a Research Networking Programme of the European Science Foundation, and FKR by the DFG via the Emmy Noether Program (RO 3676/1-1) and by the

ARCHES prize of the German Federal Ministry of Education and Research (BMBF). AJR acknowledges funding support from the Australian Research Council Centre of Excellence for All-sky Astrophysics (CAASTRO) through project number CE110001020. STO acknowledges support from the Studienstiftung des Deutschen Volkes. Funding for collaboration was provided by the DAAD/Go8 German-Australian exchange program. This research was supported by the Partner Time Allocation (Australian National University) and the National Computational Merit Allocation Schemes of the NCI National Facility at the Australian National University. Part of the simulations were carried out on the JU-GENE supercomputer at the Forschungszentrum Jülich within the Partnership for Advanced Computing in Europe (PRA042).

- 
- [1] D. Kasen, F. K. Röpke, and S. E. Woosley, *Nature* **460**, 869 (2009), 0907.0708.
  - [2] M. Kromer, S. A. Sim, M. Fink, F. K. Röpke, I. R. Seitenzahl, and W. Hillebrandt, *ApJ* **719**, 1067 (2010), 1006.4489.
  - [3] R. Pakmor, M. Kromer, S. Taubenberger, S. A. Sim, F. K. Röpke, and W. Hillebrandt, *ApJ* **747**, L10 (2012), 1201.5123.
  - [4] M. Kromer, M. Fink, V. Stanishev, S. Taubenberger, F. Ciaraldi-Schoolman, R. Pakmor, F. K. Röpke, A. J. Ruiter, I. R. Seitenzahl, S. A. Sim, et al., *MNRAS* **429**, 2287 (2013), 1210.5243.
  - [5] S. A. Sim, I. R. Seitenzahl, M. Kromer, F. Ciaraldi-Schoolmann, F. K. Röpke, M. Fink, W. Hillebrandt, R. Pakmor, A. J. Ruiter, and S. Taubenberger, *MNRAS* **436**, 333 (2013), 1308.4833.
  - [6] F. K. Röpke, M. Kromer, I. R. Seitenzahl, R. Pakmor, S. A. Sim, S. Taubenberger, F. Ciaraldi-Schoolmann, W. Hillebrandt, G. Aldering, P. Antilogus, et al., *ApJ* **750**, L19 (2012), 1203.4839.
  - [7] M. Stehle, P. A. Mazzali, S. Benetti, and W. Hillebrandt, *MNRAS* **360**, 1231 (2005), arXiv:astro-ph/0409342.
  - [8] P. A. Mazzali, K. Nomoto, K. Maeda, J. Deng, S. Benetti, F. Röpke, and W. Hillebrandt, **391**, 347 (2008).
  - [9] S. Hachinger, P. A. Mazzali, S. Taubenberger, R. Pakmor, and W. Hillebrandt, *MNRAS* **399**, 1238 (2009), 0907.2542.
  - [10] S. Hachinger, P. A. Mazzali, M. Sullivan, R. S. Ellis, K. Maguire, A. Gal-Yam, D. A. Howell, P. E. Nugent, E. Baron, J. Cooke, et al., *MNRAS* **429**, 2228 (2013), 1208.1267.
  - [11] D. Kasen, *ApJ* **708**, 1025 (2010), 0909.0275.
  - [12] J. S. Bloom, D. Kasen, K. J. Shen, P. E. Nugent, N. R. Butler, M. L. Graham, D. A. Howell, U. Kolb, S. Holmes, C. A. Haswell, et al., *ApJ* **744**, L17 (2012), 1111.0966.
  - [13] P. J. Brown, K. S. Dawson, M. de Pasquale, C. Gronwall, S. Holland, S. Immler, P. Kuin, P. Mazzali, P. Milne, S. Oates, et al., *ApJ* **753**, 22 (2012), 1110.2538.
  - [14] F. Patat, P. Chandra, R. Chevalier, S. Justham, P. Podsiadlowski, C. Wolf, A. Gal-Yam, L. Pasquini, I. A. Crawford, P. A. Mazzali, et al., *Science* **317**, 924 (2007), arXiv:0707.2793.
  - [15] A. Sternberg, A. Gal-Yam, J. D. Simon, D. C. Leonard, R. M. Quimby, M. M. Phillips, N. Morrell, I. B. Thompson, I. Ivans, J. L. Marshall, et al., *Science* **333**, 856 (2011), 1108.3664.
  - [16] B. Dilday, D. A. Howell, S. B. Cenko, J. M. Silverman, P. E. Nugent, M. Sullivan, S. Ben-Ami, L. Bildsten, M. Bolte, M. Endl, et al., *Science* **337**, 942 (2012), 1207.1306.
  - [17] I. R. Seitenzahl, S. Taubenberger, and S. A. Sim, *MNRAS* **400**, 531 (2009), 0908.0247.
  - [18] W. E. Kerzendorf, S. Taubenberger, I. R. Seitenzahl, and A. J. Ruiter, *ApJ* **796**, L26 (2014), 1406.6050.
  - [19] S. A. Sim and P. A. Mazzali, *MNRAS* **385**, 1681 (2008), 0710.3313.
  - [20] K. Maeda, Y. Terada, D. Kasen, F. K. Röpke, A. Bamba, R. Diehl, K. Nomoto, M. Kromer, I. R. Seitenzahl, H. Yamaguchi, et al., *ApJ* **760**, 54 (2012), 1208.2094.
  - [21] A. Summa, A. Ulyanov, M. Kromer, S. Boyer, F. K. Röpke, S. A. Sim, I. R. Seitenzahl, M. Fink, K. Mannheim, R. Pakmor, et al., *A&A* **554**, A67 (2013), 1304.2777.
  - [22] M. Gilfanov and Á. Bogdán, *Nature* **463**, 924 (2010), 1002.3359.
  - [23] C. Badenes, J. P. Hughes, E. Bravo, and N. Langer, *ApJ* **662**, 472 (2007), arXiv:astro-ph/0703321.
  - [24] H. Yamaguchi, C. Badenes, A. R. Foster, E. Bravo, B. J. Williams, K. Maeda, M. Nobukawa, K. A. Eriksson, N. S. Brickhouse, R. Petre, et al., *ApJ* **801**, L31 (2015), 1502.04255.
  - [25] P. Ruiz-Lapuente, F. Comeron, J. Méndez, R. Canal, S. J. Smartt, A. V. Filippenko, R. L. Kurucz, R. Chornock, R. J. Foley, V. Stanishev, et al., *Nature* **431**, 1069 (2004), arXiv:astro-ph/0410673.
  - [26] W. E. Kerzendorf, B. P. Schmidt, M. Asplund, K. Nomoto, P. Podsiadlowski, A. Frebel, R. A. Fesen, and D. Yong, *ApJ* **701**, 1665 (2009), 0906.0982.
  - [27] B. E. Schaefer and A. Pagnotta, *Nature* **481**, 164 (2012).
  - [28] A. Horesh, S. R. Kulkarni, D. B. Fox, J. Carpenter, M. M. Kasliwal, E. O. Ofek, R. Quimby, A. Gal-Yam, S. B. Cenko, A. G. de Bruyn, et al., *ApJ* **746**, 21 (2012), 1109.2912.



- [29] L. Chomiuk, A. M. Soderberg, M. Moe, R. A. Chevalier, M. P. Rupen, C. Badenes, R. Margutti, C. Fransson, W.-f. Fong, and J. A. Dittmann, *ApJ* **750**, 164 (2012), 1201.0994.
- [30] L. R. Yungelson and M. Livio, *ApJ* **528**, 108 (2000), arXiv:astro-ph/9907359.
- [31] A. J. Ruiter, K. Belczynski, and C. Fryer, *ApJ* **699**, 2026 (2009), 0904.3108.
- [32] A. J. Ruiter, K. Belczynski, S. A. Sim, W. Hillebrandt, C. L. Fryer, M. Fink, and M. Kromer, *MNRAS* **417**, 408 (2011), 1011.1407.
- [33] S. Toonen, G. Nelemans, and S. Portegies Zwart, *A&A* **546**, A70 (2012), 1208.6446.
- [34] A. J. Ruiter, S. A. Sim, R. Pakmor, M. Kromer, I. R. Seitenzahl, K. Belczynski, M. Fink, M. Herzog, W. Hillebrandt, F. K. Röpke, et al., *MNRAS* **429**, 1425 (2013), 1209.0645.
- [35] N. Mennekens, D. Vanbeveren, J. P. De Greve, and E. De Donder, *A&A* **515**, A89 (2010), 1003.2491.
- [36] X. Wang, L. Wang, A. V. Filippenko, G. Aldering, P. Antilogus, D. Arnett, D. Baade, E. Baron, B. J. Barris, S. Benetti, et al., *ApJ* **749**, 126 (2012), 1110.5809, URL <http://adsabs.harvard.edu/abs/2012ApJ...749..126W>.
- [37] C. Badenes and D. Maoz, *ApJ* **749**, L11 (2012), 1202.5472.
- [38] I. R. Seitenzahl, F. Ciaraldi-Schoolmann, F. K. Röpke, M. Fink, W. Hillebrandt, M. Kromer, R. Pakmor, A. J. Ruiter, S. A. Sim, and S. Taubenberger, *MNRAS* **429**, 1156 (2013), 1211.3015.
- [39] W. Hillebrandt and J. C. Niemeyer, *ARA&A* **38**, 191 (2000), arXiv:astro-ph/0006305.
- [40] Z.-W. Liu, R. Pakmor, I. R. Seitenzahl, W. Hillebrandt, M. Kromer, F. K. Röpke, P. Edelmann, S. Taubenberger, K. Maeda, B. Wang, et al., *ApJ* **774**, 37 (2013), 1307.5579.
- [41] I. R. Seitenzahl, G. Cescutti, F. K. Röpke, A. J. Ruiter, and R. Pakmor, *A&A* **559**, L5 (2013), 1309.2397.
- [42] I. R. Seitenzahl, A. Summa, F. Krauß, S. A. Sim, R. Diehl, D. Elsässer, M. Fink, W. Hillebrandt, M. Kromer, K. Maeda, et al., *MNRAS* **447**, 1484 (2015), 1412.0835.
- [43] F. X. Timmes and S. E. Woosley, *ApJ* **396**, 649 (1992).
- [44] H. A. Bethe, *Reviews of Modern Physics* **62**, 801 (1990).
- [45] K. Nomoto, F.-K. Thielemann, and K. Yokoi, *ApJ* **286**, 644 (1984).
- [46] T. Kunugise and K. Iwamoto, *PASJ* **59**, L57+ (2007).
- [47] A. Odrzywolek and T. Plewa, *A&A* **529**, A156 (2011), 1006.0490.
- [48] T. Plewa, *ApJ* **657**, 942 (2007), arXiv:astro-ph/0611776.
- [49] A. M. Khokhlov, *A&A* **245**, 114 (1991).
- [50] T. Plewa, A. C. Calder, and D. Q. Lamb, *ApJ* **612**, L37 (2004), arXiv:astro-ph/0405163.
- [51] I. R. Seitenzahl, C. A. Meakin, D. Q. Lamb, and J. W. Truran, *ApJ* **700**, 642 (2009), 0905.3104.
- [52] W. Hillebrandt, M. Kromer, F. K. Röpke, and A. J. Ruiter, *Frontiers of Physics* **8**, 116 (2013), 1302.6420.
- [53] F. Ciaraldi-Schoolmann, I. R. Seitenzahl, and F. K. Röpke, *A&A* **559**, A117 (2013), 1307.8146.
- [54] S. L. Shapiro and S. A. Teukolsky, *Black Holes, White Dwarfs, and Neutron Stars* (John Wiley & Sons, New York, 1983).
- [55] S. E. Woosley, *ApJ* **476**, 801 (1997).
- [56] K. Langanke and G. Martínez-Pinedo, *Atomic Data and Nuclear Data Tables* **79**, 1 (2001).
- [57] I. R. Seitenzahl, D. M. Townsley, F. Peng, and J. W. Truran, *Atomic Data and Nuclear Data Tables* **95**, 96 (2009).
- [58] N. Itoh, H. Hayashi, A. Nishikawa, and Y. Kohyama, *ApJS* **102**, 411 (1996).
- [59] T. e. Consortium, :, P. A. Seoane, S. Aoudia, H. Audley, G. Auger, S. Babak, J. Baker, E. Barausse, S. Barke, et al., *ArXiv e-prints* (2013), 1305.5720.
- [60] G. Nelemans, L. R. Yungelson, and S. F. Portegies Zwart, *A&A* **375**, 890 (2001), astro-ph/0105221.
- [61] A. J. Ruiter, K. Belczynski, S. A. Sim, W. Hillebrandt, C. L. Fryer, M. Fink, and M. Kromer (2010), 1011.1407.
- [62] M. Dan, S. Rosswog, J. Guillochon, and E. Ramirez-Ruiz, *ApJ* **737**, 89 (2011), 1101.5132.
- [63] D. Falta, R. Fisher, and G. Khanna, *Physical Review Letters* **106**, 201103 (2011), 1011.6387.
- [64] D. Falta and R. Fisher, *Phys. Rev. D* **84**, 124062 (2011), 1112.2782.
- [65] S. Kawamura, M. Ando, N. Seto, S. Sato, T. Nakamura, K. Tsubono, N. Kanda, T. Tanaka, J. Yokoyama, I. Funaki, et al., *Classical and Quantum Gravity* **28**, 094011 (2011).
- [66] K. Yagi and N. Seto, *Phys. Rev. D* **83**, 044011 (2011), 1101.3940.
- [67] L. Blanchet, T. Damour, and G. Schaefer, *MNRAS* **242**, 289 (1990).
- [68] E. Müller and H.-T. Janka, *A&A* **317**, 140 (1997).
- [69] T. Nakamura and K.-I. Oohara, *Methods in 3 D numerical relativity*. (1989), pp. 254–280.
- [70] R. Moenchmeyer, G. Schaefer, E. Müller, and R. E. Kates, *A&A* **246**, 417 (1991).
- [71] C. W. Misner, K. S. Thorne, and J. A. Wheeler, *Gravitation* (1973).
- [72] C. J. Moore, R. H. Cole, and C. P. L. Berry, *Classical and Quantum Gravity* **32**, 015014 (2015), 1408.0740.
- [73] E. Müller, *A&A* **114**, 53 (1982).
- [74] E. Müller, H.-T. Janka, and A. Wongwathanarat, *A&A* **537**, A63 (2012), 1106.6301.